Coordinated Power Control for Autonomous Power Balancing of Offshore Wind-Hydrogen Systems

Chunjun Huang
Dept. of Electrical Sustainable Energy
Delft University of Technology
Delft, The Netherlands
C.J.Huang@tudelft.nl

Xin Jin
Dept. of Energy and Process Engineering
Norwegian University of Science and Technology
Trondheim, Norway
xin.jin1@ntnu.no

José Luis Rueda Torres
Dept. of Electrical Sustainable Energy
Delft University of Technology
Delft, The Netherlands
J.L.RuedaTorres@tudelft.nl

***Abstract*—Offshore wind-hydrogen energy systems (OWHESs) enable large-scale renewable integration and green hydrogen production, playing a pivotal role in the clean energy transition. However, their stable operation critically depends on maintaining internal power balance. This paper addresses the challenge of achieving autonomous coordination of co-located wind-hydrogen plants within OWHES to prevent local power fluctuations from propagating to the offshore network. A coordinated active power control framework is proposed, allowing the co-located plant to operate as a self-balancing unit. The approach employs wind power de-loading to absorb surpluses and electrolyzer load reduction to mitigate deficits, with an intelligent switching mechanism ensuring seamless transitions between control modes. A 2-GW OWHES digital model is built on a commercial real-time simulator to demonstrate the proposed method. Real-time simulation results demonstrate that the proposed control effectively eliminates internal imbalances of the co-located plant, maintaining zero net power exchange with the external offshore network under varying wind and electrolyzer load conditions, thereby ensuring stable nominal power delivery through the HVDC link to onshore systems.**

***Index Terms*—Offshore wind energy, HVDC transmission, electrolyzer, power balance control, system stability.**

I. Introduction

As the global clean energy transition accelerates, offshore wind power has become a cornerstone technology for large-scale, carbon-free electricity generation. Ambitious national targets, such as the Netherlands' 30-40 GW goal by 2040 [1], underscore its pivotal role in future energy systems. Achieving such large-scale renewable integration requires advanced transmission solutions, with high-voltage direct current (HVDC) systems based on modular multilevel converters (MMCs) offering efficient and controllable power transfer [2]. However, building a resilient offshore energy system goes beyond power transmission; it also demands effective energy storage and sector coupling to manage variability and enhance flexibility. In this context, green hydrogen has emerged as a key energy carrier. The integration of multi-gigawatt power-to-hydrogen facilities within offshore hubs, forming offshore wind-hydrogen energy systems (OWHES), is rapidly gaining momentum, especially across the North Sea region [3]. These integrated systems can mitigate wind power variability while enabling large-scale green hydrogen production.

The stability of emerging OWHES relies on efficient and fast power balance management among converter-interfaced devices, including wind generators, HVDC systems, and electrolyzers. A defining feature of the OWHES architecture is the modular, co-located wind–hydrogen plant [4], [5]. While this modularity enhances scalability, any internal mismatch between power generation and hydrogen consumption can propagate disturbances to the offshore network. Without proper power management and coordination, such fluctuations may overload HVDC links and compromise overall system stability.

To address these challenges, this paper proposes a coordinated active power control framework that enables co-located wind–hydrogen plants to operate autonomously as self-balancing units. The framework employs a high-level supplementary power control structure with an intelligent switching mechanism that dynamically coordinates wind power de-loading and electrolyzer load curtailment to maintain internal power equilibrium. The proposed method is implemented and demonstrated on a 2 GW OWHES digital model developed in a commercial real-time digital simulator (RTDS) platform through electromagnetic transient (EMT) simulations.

II. Offshore Wind-Hydrogen Energy System

A. System Description

Fig. 1 shows the detailed topology of the studied OWHES, representing a 2 GW integrated offshore hub designed for both power export and on-site hydrogen production. The system employs a symmetric bipolar HVDC link capable of transmitting 2 GW of power from the offshore system to the onshore system. Offshore generation totals 2.5 GW, comprising four 500 MW main WPPs for bulk power export and two identical 250 MW co-located wind–hydrogen plants combining a wind power plant (WPP) and an electrolyzer plant (ELP). The WPPs and ELPs operate under their own primary control schemes to ensure local stability. In the WPPs, Type-IV wind turbines extract maximum power through maximum power point tracking (MPPT) control on the machine-side converter (MSC), while the grid-side converter (GSC) maintains the turbine's

The research work has received funding from TenneT TSO B.V within the FUTURESYSTEM research project "Adaptive fast active power control for stabilization of multi-converter dynamics in offshore electrical energy-hydrogen hubs". It reflects only the authors' views, and the aforesaid organization is not responsible for any use that may be made of the paper's content.

Corresponding author: José L. Rueda Torres (J.L.RuedaTorres@tudelft.nl).

979-8-3315-8138-1

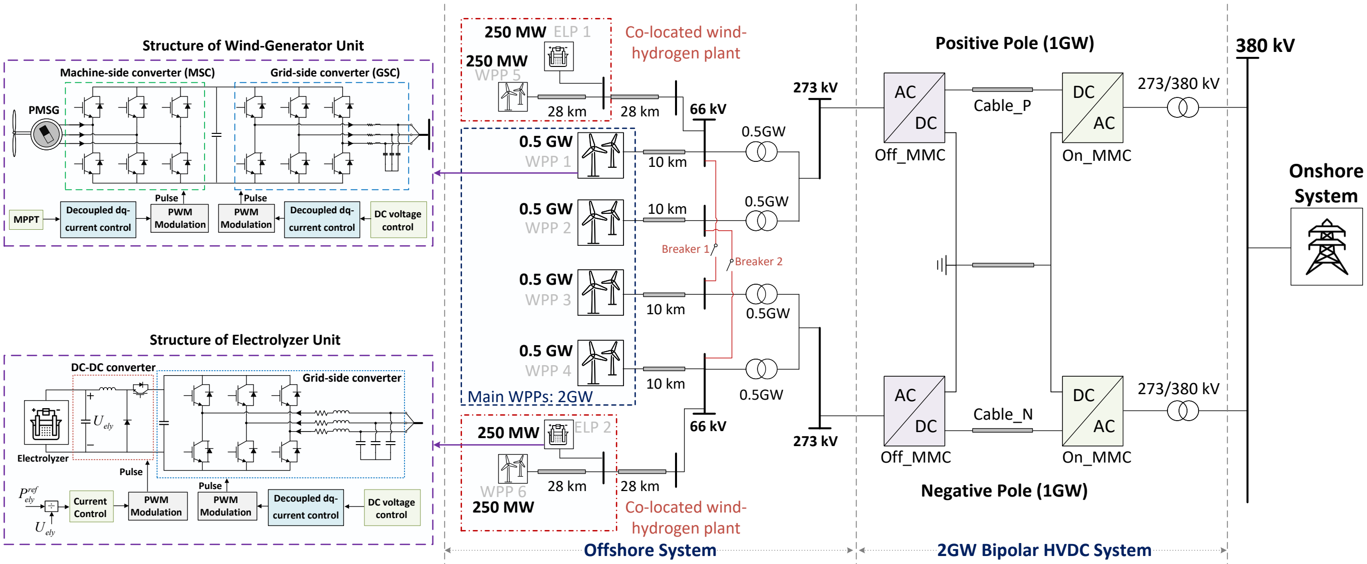

Fig. 1. Topology of the updated offshore wind-hydrogen energy system

DC-link voltage [6]. Each ELP includes a GSC regulating its local DC-link voltage and a DC–DC converter controlling the electrolyzer's active power consumption according to the high-level setpoint (P_{ely}^{ref}) [7].

Particularly, the intended operation of each co-located plant is autonomous and self-sufficient: the 250 MW WPP output is entirely consumed by its associated ELP, ensuring zero active power exchange with the external offshore network.

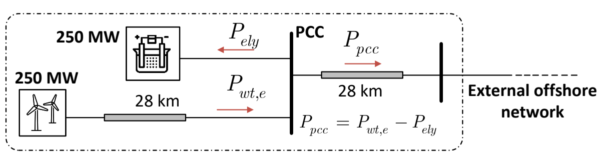

Fig. 2. Schematic of power flow within the co-located wind-hydrogen plant

B. Control Objective of Co-located Wind-Hydrogen Plant

While the primary controllers ensure local stability of individual components, they do not inherently coordinate power balance at the plant level. This leads to the core challenge: the absence of a built-in self-balancing mechanism. For example, a sudden drop in wind speed leaves the electrolyzer under-supplied, causing it to draw power from the offshore network. Conversely, a reduction in electrolyzer load leads to surplus wind power being injected into the offshore network. Both situations violate the autonomy principle and disturb the overall system.

Therefore, the key objective of this study is to design an advanced active power control strategy that enforces this autonomy, ensuring that the point of common coupling (PCC) power exchange of the co-located plant remains near zero under internal fluctuations. According to Fig. 2, this objective can be expressed as:

$$P_{pcc} = P_{wt,e} - P_{ely} = 0 \tag{1}$$

where $P_{wt,e}$ and P_{ely} denote the electrical power generated by the WPP and consumed by the ELP, respectively.

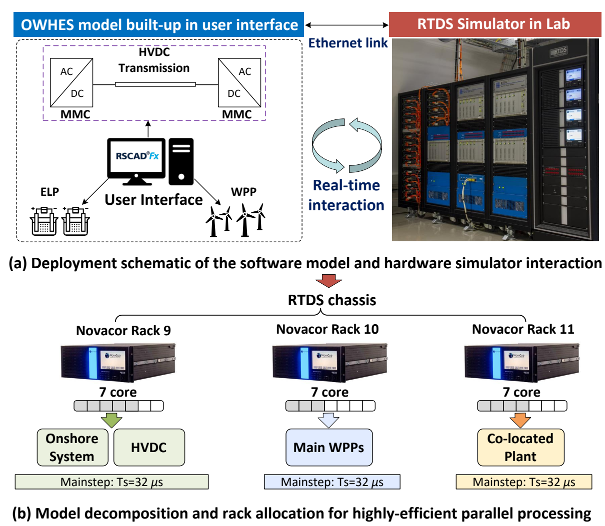

Fig. 3. Implementation of the digital OWHES model on the RTDS platform

C. Real-Time Simulation Platform

Analyzing the fast dynamic interactions of a gigawatt-scale OWHES and the demonstration of any advanced control strategy requires a high-fidelity, real-time simulation environment. To this end, an EMT digital model of the entire 2-GW OWHES is developed and deployed on a real-time digital simulator (RTDS) platform. The deployment architecture of this digital model is illustrated in Fig. 3. As shown in Fig. 3(a), the system model is first constructed within the RSCAD software user interface. This model is then deployed onto the physical RTDS Simulator hardware in the laboratory via an Ethernet link. This setup facilitates a continuous, closed-loop interaction between

979-8-3315-8138-1

the software environment (for control and monitoring) and the hardware platform (for real-time execution), enabling a proper simulation of the system's real-time dynamics.

To handle the substantial computational load, the model is partitioned across three 7-core racks in a NovaCor chassis, as shown in Fig. 3(b): one dedicated to the bipolar HVDC link and onshore system, another to the four main WPPs, and the third to the two co-located wind–hydrogen plants. This parallel processing structure allows the entire EMT-scale digital model to run in real-time with a 32 μs time step, offering an effective platform for demonstrating the proposed control strategy.

III. Coordinated Control Framework for Co-Located Plant Autonomy

To achieve autonomous power balancing in the co-located plant, this paper proposes a coordinated control framework. As shown in Fig. 4(a), the framework consists of two supplementary power controllers for WPP and ELP respectively, and an automatic switching mechanism that governs their operation.

A. Supplementary Controller Design and Principles

The supplementary controllers are designed to manage power surpluses and deficits within the co-located plant by actively adjusting the operating points of the WPP and ELP. Both controllers adopt a PI structure to eliminate the steady-state error of the PCC power exchange (P_{pcc}), with a reference set as $P_{ref} = 0$. The framework's operation is founded on a predefined control priority based on the physical capabilities of the assets. The WPP is designated as the primary actuator for resolving power surpluses ($P_{pcc} > 0$), leveraging its inherent flexibility to reduce output by moving away from the MPPT curve. Conversely, the ELP acts as the secondary actuator, used only to resolve power deficits ($P_{pcc} < 0$). This latter case is specifically triggered when the WPP is power-limited by low wind speed and cannot increase its generation.

1) WPP Controller for Power Surplus Management: The WPP supplementary controller generates an adjustment torque signal, T_{wt}, according to the control law:

$$T_{wt}(t) = K_p^{wt}(P_{ref} - P_{pcc}(t)) + K_i^{wt} \int (P_{ref} - P_{pcc}(t))dt \tag{2}$$

where K_p^{wt} and K_i^{wt} are the PI controller gains. This signal then modifies the standard MPPT power reference to formulate the final command for the turbine's MSC:

$$P_{msc}^{ref} = P_{MPPT} + T_{wt} \cdot \omega_{wt} = K_{opt}\omega_{wt}^3 + T_{wt} \cdot \omega_{wt} \tag{3}$$

The controller achieves power reduction by leveraging the rotor dynamics of the wind turbine:

$$J\omega_{wt}\frac{d\omega_{wt}}{dt} = P_{wt,m} - P_{wt,e} \tag{4}$$

where J is the rotor's moment of inertia. As illustrated in Fig. 4(b), when a power surplus occurs (e.g., due to a drop in electrolyzer load), the desired new equilibrium is at a lower power level (Point D). To transition from the initial MPPT state (Point A) to Point D, the controller strategically manipulates P_{msc}^{ref} based on (3). This action induces a temporary imbalance between the mechanical power ($P_{wt,m}$) and electrical power ($P_{wt,e}$). Driven by the rotor dynamics (4), the turbine subsequently adjusts its operating point along the A–B–C–D trajectory until a new steady equilibrium is established.

2) ELP Controller for Power Deficit Management: As illustrated in Fig. 4(c), a drop in wind speed forces the turbine's operating point down its MPPT curve from A to B, reducing the available power. To counteract the resulting power deficit at the PCC, the ELP supplementary controller generates an adjustment power signal, ΔP_{ely}^{ref}:

$$\Delta P_{ely}^{ref}(t) = K_p^{ely}(P_{ref} - P_{pcc}(t)) + K_i^{ely} \int (P_{ref} - P_{pcc}(t))dt \tag{5}$$

where K_p^{ely} and K_i^{ely} are the PI controller gains. This signal modifies the electrolyzer's original operating point, $P_{ely,1}^{ref}$, to produce the final command for its DC-DC converter:

$$P_{ely}^{ref} = P_{ely,1}^{ref} + \Delta P_{ely}^{ref} \tag{6}$$

This action dynamically curtails the electrolyzer's consumption to precisely match the available generation at the new equilibrium point (Point B).

B. Automatic Coordination and Switching Logic

A proper coordination mechanism between the two controllers is essential to manage them and enforce the control priority without conflict. This is achieved through the automatic switching mechanism, depicted in Fig. 4(a) and summarized in Table I. The mechanism leverages the PI controller outputs as state indicators to govern an S-R flip-flop, which in turn defines the activation signal K (for WPP) and G (for ELP).

The logic operates through three distinct phases. *1) Default or Surplus State:* The WPP controller remains active by default, or whenever a power surplus occurs ($K = 1, G = 0$), to handle any potential power surplus. *2) Deficit Detection:* A power deficit, occurring when the WPP is power-limited, forces its PI output T_{wt} to transition to a negative value. This negative-going transition sets the flip-flop ($Q = 1$), seamlessly activating the ELP controller ($K = 0, G = 1$). *3) Recovery:* A subsequent power surplus during wind speed recovery causes the active ELP controller's output ΔP_{ely}^{ref} to become positive, which resets the flip-flop ($Q = 0$) and autonomously hands control back to the WPP.

Crucially, to ensure a smooth transition, signals K, G are also used for resetting PI controllers. Whenever a controller is deactivated, its PI integrator is simultaneously reset. This key feature prevents integrator windup and guarantees a smooth transfer of control between the two modes. This coordinated logic guarantees a decisive and fully autonomous switching, ensuring robust power balance under changing conditions.

IV. Case Study

A. Baseline Scenario: Risk of Uncoordinated Operation

To highlight the necessity of coordination, a baseline scenario is first simulated where the 250 MW ELP (ELP2) within

979-8-3315-8138-1

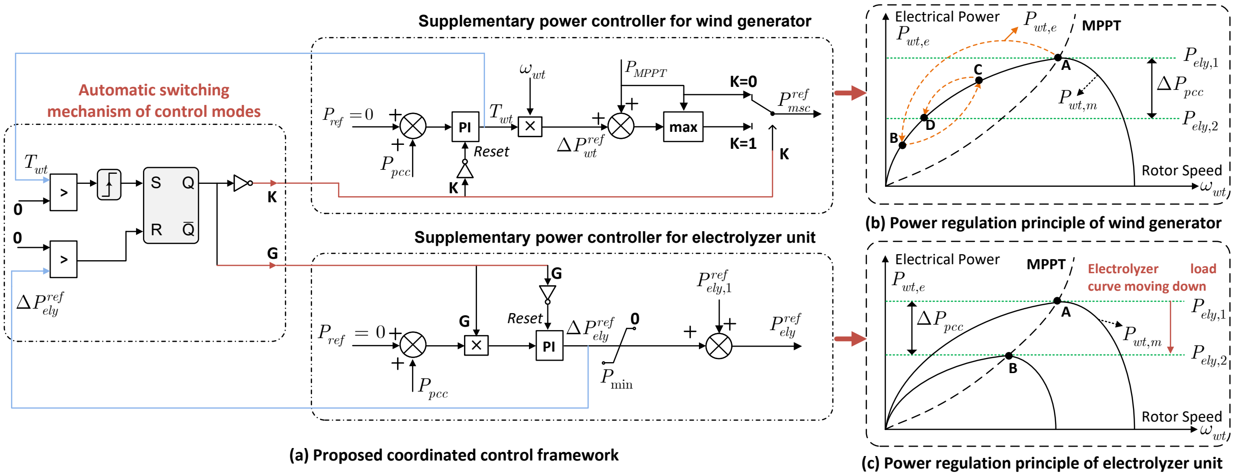

Fig. 4. Proposed coordinated control framework and power regulation principle for the co-located wind-hydrogen plant.

TABLE I
LOGIC OF THE AUTOMATIC SWITCHING MECHANISM

Condition	Trigger Signal	State (Q)	Active Controller
Power Balance	$T_{wt} \approx 0$	0	WPP (Primary)
Power Surplus	$T_{wt} > 0$	0	WPP (Primary)
Power Deficit	$T_{wt} < 0$	1 (Set)	ELP (Secondary)
Recovery	$\Delta P_{ely}^{ref} > 0$	0 (Reset)	WPP (Primary)

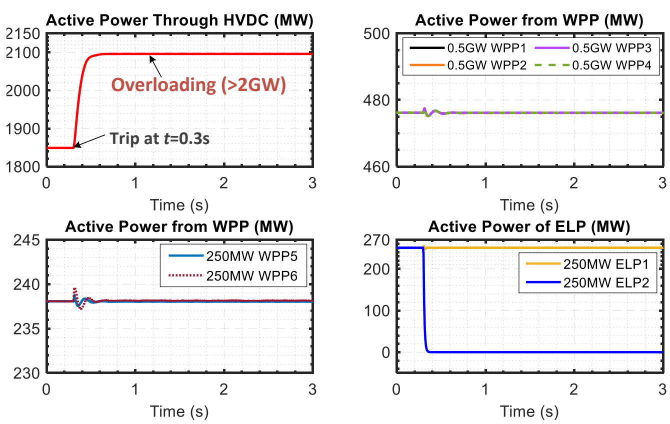

Fig. 5. OWHES active power response under an ELP load loss.

a co-located plant undergoes an abrupt trip at $t = 0.3$ s. Without the proposed control, the co-located WPP continues to operate in MPPT mode. As shown in Fig. 5, the sudden loss of load causes the WPP's surplus power to be instantaneously injected into the offshore network. This power surge is directly reflected in the HVDC link's throughput, which rises sharply from its nominal 1850 MW to over 2000 MW, resulting in a sustained and unacceptable overload. This scenario clearly demonstrates that uncoordinated operation poses a severe risk to the transmission infrastructure and overall system stability, highlighting the critical need for autonomous power balancing.

B. Coordinated Control During Electrolyzer Load Variation

The framework's capability to handle load-side disturbances is assessed through two test cases involving step changes in electrolyzer power demand, as shown in Fig. 6.

In the first case, depicted in Fig. 6(a), the ELP load is reduced from 1.0 p.u. (250 MW) to 0.5 p.u. (125 MW) at $t = 6$ s, creating a power surplus. The WPP supplementary controller detects this surplus and smoothly de-loads the turbine by shifting its operating point away from the MPPT curve (Point A). Wind power quickly converges to a new level (Point D), precisely matching the reduced ELP load, and the PCC power exchange returns to zero within about 24 s. In the second case, shown in Fig. 6(b), the ELP load increases from 0.5 p.u. to 0.8 p.u. (200 MW) at $t = 6$ s. The controller promptly identifies the resulting power deficit and releases the de-loading margin, enabling the WPP to ramp up its output. The system again re-establishes internal power equilibrium (P_{pcc} returning to zero) after a transient of about 24 s.

These results verify the framework's bidirectional capability to manage both surplus and deficit events on the load side, actively eliminating internal imbalances within co-located plants.

C. Coordinated Control During Wind Speed Variation

The controller's performance under generation-side fluctuations is further demonstrated through a complete low-wind event cycle, as presented in Fig. 7.

The first scenario, shown in Fig. 7(a), simulates a low-wind event at $t = 6$ s, where the WPP's available power drops to 100 MW. The automatic switching logic instantly detects the resulting power deficit and activates the ELP supplementary controller ($G = 1$). The results show that the ELP's power consumption is smoothly and rapidly curtailed, precisely tracking the declining power generation from the WPP. Consequently, instead of a large power import, after a 24-second transient, P_{pcc} is kept within around zero, preventing any significant strain on the external network.

The recovery scenario is depicted in Fig. 7(b). Starting from the curtailed state, the wind speed increases at $t = 6$ s, causing

979-8-3315-8138-1

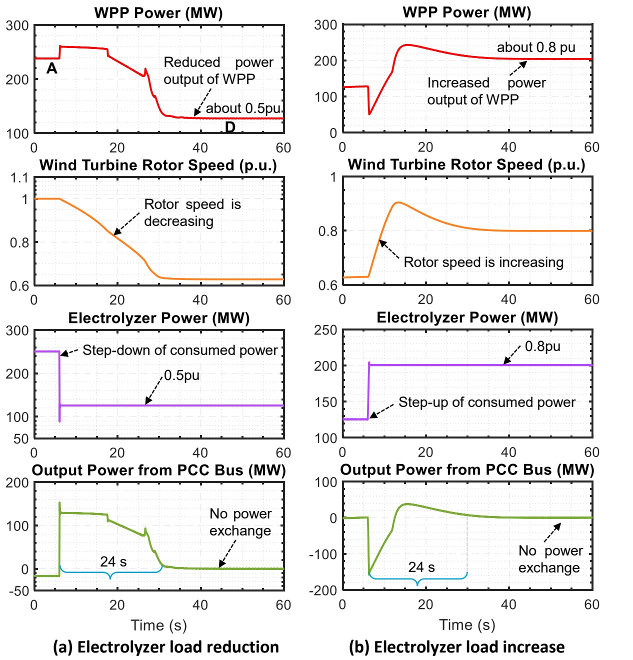

Fig. 6. System response with the coordinated control under electrolyzer load variations: (a) Step-down in ELP load; (b) Step-up in ELP load.

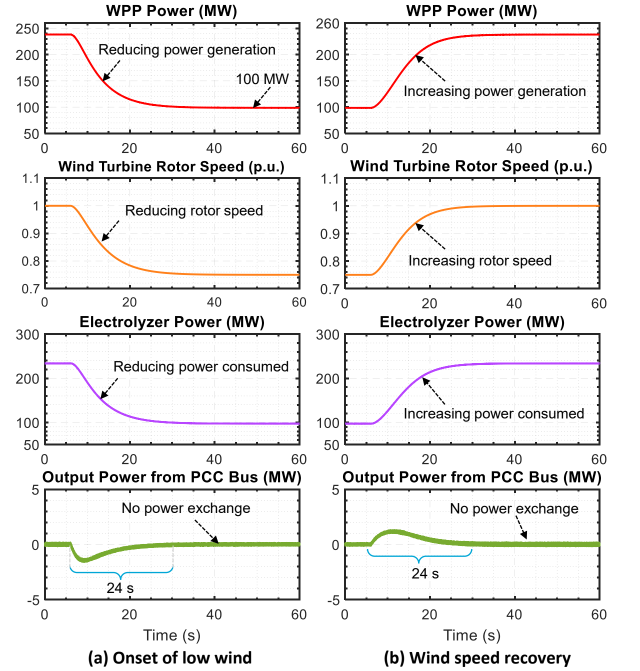

Fig. 7. System dynamic response with the coordinated control during a low-wind event cycle: (a) Onset of low wind ; (b) Wind speed recovery.

the available power from the WPP to rise and creating a momentary power surplus. The switching logic detects this and autonomously hands control back to the WPP controller ($K = 1$). The results show the ELP seamlessly ramping its consumption back up towards its nominal rating. Simultaneously, the WPP's power output increases as its rotor re-accelerates towards the optimal MPPT speed. During this recovery transition, the WPP supplementary controller actively manages the transient power surplus, ensuring that the P_{pcc} remains tightly regulated around zero. After a similar 24-second transient, the system returns to its nominal, self-balanced operating state.

These results confirm that the proposed coordinated control framework enables the co-located wind–hydrogen plant to operate as a fully autonomous unit, effectively mitigating both load- and generation-induced power disturbances.

V. Conclusion

This paper proposes a coordinated active power control framework to ensure the autonomous operation of co-located wind-hydrogen plants within a large-scale OWHES. By developing supplementary controllers for wind power de-loading and electrolyzer load curtailment, governed by an intelligent automatic switching mechanism, the framework enables each co-located plant to achieve perfect self-balancing. Real-time simulations on a 2-GW OWHES digital model demonstrate the substantial risk of HVDC overloading under uncoordinated operation. In contrast, the proposed framework proves highly effective, eliminating internal power imbalances caused by both load- and generation-side disturbances. It maintains a near-zero net power exchange at the PCC for co-located plants, preventing any adverse impact on the main offshore network.

The results confirm that the proposed framework allows the co-located plant to function as an autonomous, grid-friendly unit, enhancing the stability and resilience of future modular OWHES. Future work will extend this concept to incorporate ancillary services, such as fast frequency regulation through advanced AI-driven optimization methods, to further enhance the flexibility and economic performance of large-scale offshore wind-hydrogen energy systems.

References

[1] Ministry of Climate Policy and Green Growth, "Offshore Wind Energy Action Plan," Tech. Rep., 2025. [Online]. Available: https://english.rvo.nl/sites/default/files/2025-09/Offshore-Wind-Energy-Action-Plan-Letter-to-Parliament.pdf

[2] A. Alassi, S. Bañales, O. Ellabban, G. Adam, and C. MacIver, "Hvdc transmission: Technology review, market trends and future outlook," *Renewable and Sustainable Energy Reviews*, vol. 112, pp. 530–554, 2019.

[3] North Sea Wind Power Hub, "Offshore Energy Hubs: Blueprints with Offshore Electrolysis," 2024.

[4] V. Timmers, A. Egea-Àlvarez, A. Gkountaras, and L. Xu, "Control and power balancing of an off-grid wind turbine with co-located electrolyzer," *IEEE Transactions on Sustainable Energy*, vol. 15, no. 4, pp. 2349–2360, 2024.

[5] Z. Wang, Y. Tang, C. Shi, and L. Guo, "Power balance control of an energy-storage-free islanded offshore wind hydrogen production system," *Electric Power Systems Research*, vol. 245, p. 111558, 2025.

[6] A. Honrubia-Escribano, E. Gómez-Lázaro, J. Fortmann, P. Sørensen, and S. Martin-Martinez, "Generic dynamic wind turbine models for power system stability analysis: A comprehensive review," *Renewable and Sustainable Energy Reviews*, vol. 81, pp. 1939–1952, 2018.

[7] M. B. Hossain, M. R. Islam, K. M. Muttaqi, D. Sutanto, and A. P. Agalgaonkar, "Dynamic electrical circuit modeling of a proton exchange membrane electrolyzer for frequency stability, resiliency, and sensitivity analysis in a power grid," *IEEE Transactions on Industry Applications*, vol. 59, no. 6, pp. 7271–7281, 2023.

979-8-3315-8138-1